Article

Application of Artificial Neural Networks for Accuracy Enhancements of Real-Time Flood Forecasting in the Imjin Basin

Aida Jabbari and Deg-Hyo Bae *

Department of Civil & Environmental Engineering, Sejong University, 98 Gunja-Dong, Gwangjin-Gu, Seoul 143-747, Korea; ajabbari@sju.ac.kr

* Correspondence: dhbae@sejong.ac.kr

Abstract: Hydrometeorological forecasts provide future flooding estimates to reduce damages. Despite the advances and progresses in Numerical Weather Prediction (NWP) models, they are still subject to many uncertainties, which cause significant errors forecasting precipitation. Statistical postprocessing techniques can improve forecast skills by reducing the systematic biases in NWP models. Artificial Neural Networks (ANNs) can model complex relationships between input and output data. The application of ANN in water-related research is widely studied; however, there is a lack of studies quantifying the improvement of coupled hydrometeorological model accuracy that use ANN for bias correction of real-time rainfall forecasts. The aim of this study is to evaluate the real-time bias correction of precipitation data, and from a hydrometeorological point of view, an assessment of hydrological model improvements in real-time flood forecasting for the Imjin River (South and North Korea) is performed. The comparison of the forecasted rainfall before and after the bias correction indicated a significant improvement in the statistical error measurement and a decrease in the underestimation of WRF model. The error was reduced remarkably over the Imjin catchment for the accumulated Mean Areal Precipitation (MAP). The performance of the real-time flood forecast improved using the ANN bias correction method.

---

1. Introduction

Climate change has increased extreme rainfall events, and as a result, damage from floods has significantly increased. Heavy rainfalls occurring over different areas often lead to various flooding problems. Therefore, societies need to improve flood risk management. Hydrometeorological forecasts provide future estimates to reduce damage and provide warnings of extreme events. Coupling numerical weather prediction (NWP) and hydrological models allows meteorology and hydrology connection to generate real-time flood forecasting. Real-time flood forecasting has been investigated worldwide in previous studies using hydrometeorological data [1–3].

Although NWP models have improved significantly, the restrictions of the physical processes in NWP models lead to unavoidable errors in the forecasting of meteorological properties due to nonlinearity and the chaotic atmospheric system. In analyses of the accuracy of the forecasted values of atmospheric models, the most frequent errors are related to the model error, initialization, boundary conditions of atmosphere, land and sea surface, model formulation and model parametrization during the forecast period [4]. These errors influence the output of the meteorological models.

NWP models are restricted to representing the physical processes of the chaotic atmosphere. A precise forecast of precipitation is one of the challenges of NWP models. The biased output

of these models is still a concern for hydrometeorological prediction studies [5]. NWP models are subject to many uncertainties, which cause significant errors in the forecasting of real-time precipitation. In coupled hydrometeorological studies, one critical issue before running a rainfall-runoff model is to reduce the input forcing errors that are produced by the meteorological model. Therefore, postprocessing of the model outputs of the real-time forecast data would result in a better match with the observation records. Statistical postprocessing methods improve real-time forecast accuracy by relating the model outputs to the observed values.

Several studies have shown that statistical postprocessing improved forecast performance by reducing systematic biases [6,7]. The main purpose of statistical bias correction is to develop a relationship between the modeled and observed data. Commonly used statistical methods are the quantile-based mapping method [8] and regression approaches that include linear relationships [9] and nonlinear relationships [10]. In real-time flood forecasting, a comparison of different postprocessing methods such as Bayesian Model Averaging (BMA), classic poor man ensemble (PME) and Multimodel SuperEnsemble Dressing (MSD) indicated that the MSD approach provided better precipitation data for floods in Italy [11]. Six different bias correction methods (including linear scaling (LS), local intensity scaling (LOCI) scaling, Daily Translation (DT), daily bias correction (DBC), quantile mapping based on an empirical distribution (QME) and quantile mapping based on a gamma distribution (QMG)) were applied in ten North American river basins to determine the sensitivity of the bias correction methods on climate models [12]. All bias correction methods improve the precipitation forecasts, but DT, DBC, QME, and QMG resulted in the most significant improvements to the simulations [12].

An Artificial Neural Network (ANN) can predict and modeling input and output data [5]. ANN is more practical than other techniques due its ability to handle complex nonlinear systems. In previous studies, ANN was applied for various purposes such as precipitation estimation [13–15], hydrological modeling [16–19], hydrometeorological studies [20,21], flood forecasting [22–24] and flood inundation [25,26]. Three new hybrid artificial intelligence optimization models (adaptive neuro-fuzzy inference system (ANFIS) with cultural (ANFIS-CA), bees (ANFIS-BA), and invasive weed optimization (ANFIS-IWO) algorithms) were presented for flood susceptibility mapping in Iran. The results showed that ANFIS-IWO had better performance and ANFIS-BA exhibited the better prediction capability [27]. The application of ANN for the prediction of water resource variables has been reviewed in 43 papers [28]; in addition, 210 papers (from 1999 to 2007) in which ANN was developed for river flow prediction including quantity and quality were reviewed [29]. ANN was applied to predict seasonal rainfall for the next 5 years and a multilayer neural network to predict rainfall time series was employed successfully in India [30]. The bias correction of the climate modeled temperature and precipitation was carried out using ANN over northern South America; compared with linear regression, ANN had a superior performance [5]. Recent reviews on the application of ANN have been reported in [31].

There is a lack of studies in the literature on the quantification of the accuracy improvement of coupled hydrometeorological models using ANN for the bias correction of real-time rainfall forecasts. The aim of this study is to evaluate the real-time bias correction of precipitation data from a hydrometeorological point of view. In addition, an assessment of forecast improvements to hydrological models that result in real-time flood forecasting of coupled hydrometeorological models is performed. To accomplish this aim, a variety of tests are conducted to quantify the accuracy assessment of real-time precipitation and flood forecasts using coupled hydrometeorological models. The present study provides details regarding the real-time precipitation accuracy improvement in addition to the forcing of the bias-corrected rainfall as input to the hydrological model. An evaluation of the accuracy enhancement of real-time flood forecasting of hydrometeorological models is also given.

2. Study Area and Data

2.1. Imjin Basin

The target area for this study is the Imjin River basin, which passes through the demilitarized zone (DMZ) in North and South Korea between 37°44′23″ N 126°31′19″ E and 39°11′12″ N 127°36′21″ E. The length and the area of the Imjin River watershed are 273.5 km and 8139 km^2, respectively. In addition, 62.9% of the area of the basin is in North Korea, and the other 37.1% is in South Korea. Because approximately two-thirds of the Imjin River is in North Korea, it is considered a transboundary river. Details regarding the study catchment are mapped in Figure 1. The source of the Imjin River is in North Korea, it then passes through South Korea where it joins the Han River, and it finally empties into the Yellow Sea. The Imjin River has complex topography with an altitude range from 155 m to 1570 m with a mean elevation of 680.5 m above mean sea level. The average annual rainfall is approximately 1100 mm, which mostly occurs during the late summer and fall [32]. The study area consists of 38 sub-basins that are defined by characteristics such as elevation, direction of the streamflow and soil conditions of the entire basin.
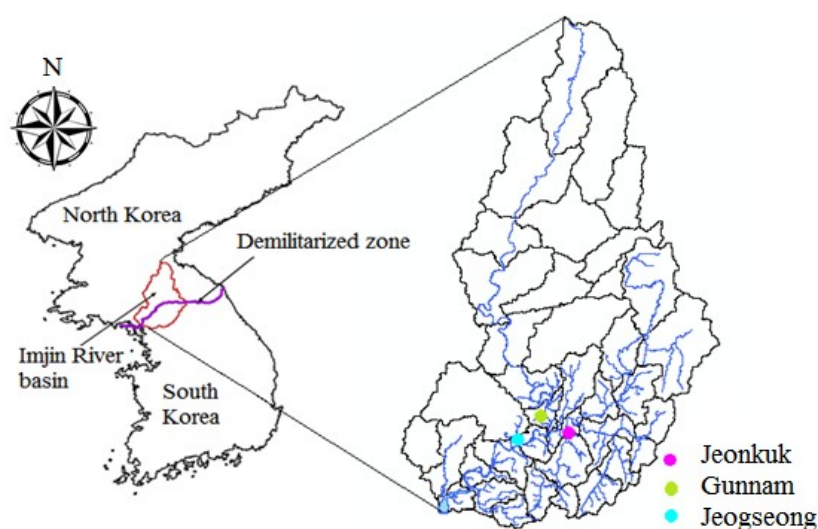
Figure 1. Location, sub-basins, river network and water level gauging stations of the Imjin River basin.

2.2. Hydrological and Meteorological Data

The Imjin River has experienced various flash floods during past years. The most extreme events are selected for consideration for flood forecasting in the Imjin River basin. In 2002, Typhoon Rusa ripped through South Korea in the Gangneung area between 31 August and 1 September, affecting the eastern and southern parts of Korea with almost 1000 mm of rainfall in 30 h [33,34]. The typhoon caused the submergence of 9000 houses and killed 113 people. In 2002 event, continuous low and high humid east wind led to the creation of frontal precipitation by cold air [34]. In 2007, Typhoon Wipha in North Korea brought heavy rain between 7–14 August and 18–20 September. Approximately 500–700 mm of rainfall caused flooding in North Korea for seven days. The westward-travelling Typhoon Wipha in 2007, caused heavy frontal precipitation was accompanied by strong wind that was developed by mesoscale disturbances in China [35]. On July 27, 2011 heavy rainfall led to extreme flooding in Seoul, South Korea. In Seoul, as a mega city with a high population concentration, 536 mm of rainfall over three days resulted in severe damage, 980 flood victims, 62 people reported as dead or missing and 19,215 inundated houses [36]. The conventional rainfall in 2011 was developed by convective systems which moved from the Yellow Sea to Seoul [37]. The percentage of the liquid precipitation in the study period was 100%.

The estimated flood damage costs due to intense rainfall events indicate the need for integrated flood management for disaster prevention. This is especially important for two countries with different natural environments, national defenses, and political problems. The Imjin River is the

seventh longest river in the Korean peninsula and encountered severe flooding during past years. Therefore, the hydrological and meteorological models are coupled to provide information to prepare for severe events, provide early alerts for imminent disasters and to minimize the flood induced hazards in this important area. Other applications of the flood forecasting system are primarily related to military operations. The Imjin River basin has a military region named Paju-si, which includes river-crossing operations. Flood hazards directly influence military operations and require the use of detailed and widely applicable hydrological models.

In this study, hydrometeorological components are coupled for real-time rainfall-runoff forecasting for the transboundary Imjin River. The observation data used in this study underwent a quality control procedure, which verified the values and filled in any missing values by the Inverse Distance Weighting (IDW) method, to complete the hourly data from at all stations.

The IDW formula is as follows:

$$R(s_0) = \sum_{i=1}^{n} w_i \times R(s_i) \tag{1}$$

$$w_i = \frac{d_{i0}^{-2}}{\sum_{i=1}^{1} d_{i0}^{-2}} \tag{2}$$

where $R(s_0)$ is the revised rainfall (mm) at s_0, $R(s_i)$ is the observed rainfall (mm) at s_i, n is the number of observed stations, w_i is the weight of s_i and d_{i0} is distances from the points to the point estimated. IDW is a deterministic spatial interpolation and one of the most popular methods of interpolation.

3. Methodology

3.1. WRF Model

The WRF model has been developed as a mesoscale model for research and operational NWP model studies. The WRF model can be used for different aspects of atmospheric and operational forecasting research at various scales such as forecasting extreme events and is especially useful for heavy rainfall predictions at a high spatial resolution [38,39]. The WRF model is a very useful tool for numerical weather predictions and data assimilation in estimating meteorological data such as rainfall, solar radiation, temperature, dew point, and wind speed by reproducing climate features at ultrafine temporal and spatial resolutions [40].

The initial and boundary conditions were obtained using external sources, such as the static geographic data provided by the United States Geological Survey (USGS) and Moderate Resolution Imaging Spectroradiometer (MODIS) data set and the gridded data provided by regional and global models including the North American Mesoscale Forecast system (NAM) and the Global Forecast System (GFS) [41]. The weather charts employed in this study were provided by the National Centers for Environmental Prediction (NCEP) Final Analysis (FNL) and have a resolution of $1° \times 1°$. In summary, using the definitions of all computational grids, geogrid interpolates terrestrial time-invariant fields, then Ungrib extracts the meteorological fields from the GRidded Information in Binary (GRIB) formatted files, and Metgrib horizontally interpolates the meteorological data to the simulation domains. Time-splitting techniques are used by the Advanced Research WRF (ARW) solver to integrate the fully compressible nonhydrostatic equations of motion. The Euler equations are in flux form and are formulated using a terrain that follows mass vertical coordinates. Finally, the second- or third- order Runge-Kutta method is applied for time-split integration [41].

In this study, WRF version 3.5.1 was applied to perform real-time forecasting of the meteorological data by using the WRF Double-Moment 6-Class (WDM6) microphysical scheme. The WRF model provided an ultrafine scale of temporal and spatial resolution (10 min and 1 km $\times$ 1 km respectively) that covers Korea and the surrounding region. The real-time forecast data had a 10-min temporal

resolution over a 72-h time series which was repeated every 6 h. The schematic construction of the real-time forecast of the WRF model is shown in Figure 2.
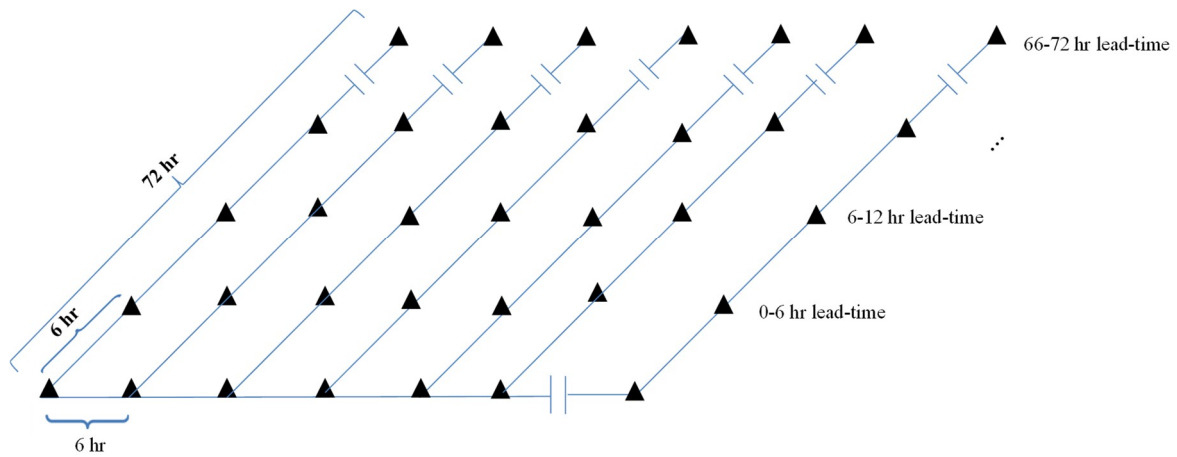
Figure 2. The schematic construction of the real-time forecast of the WRF model.

3.2. Sejong University Rainfall-Runoff (SURR) Model

The SURR model was developed by the Water Resource and GIS Laboratory, Sejong University [42] and is based on the event-oriented storage function model (SFM) by [43]. The SURR considers the rainfall loss using a soil moisture accounting model for streamflow simulation and prediction. The SURR is a semi-distributed continuous rainfall-runoff model that uses physical foundations to estimate the hydrological components including soil moisture and surface, lateral and groundwater in conjunction with the basin and channel routing to simulate the runoff. The governing equations of the SURR model for flow generation are as follows.

$$\frac{dS_{sb}(t)}{dt} = Q_{sur}(t) + Q_{lat}(t) + Q_{gw}(t) \tag{3}$$

$$Q_{sur}(t) = (Q'_{sur}(t) + Q_{surstor}(t-1))(1 - \exp[-surlag]) \tag{4}$$

$$Q_{lat}(t) = (Q'_{lat}(t) + Q_{latstor}(t-1))(1 - \exp[-latlag]) \tag{5}$$

$$Q_{gw}(t) = Q_{gw}(t-1)\cdot \exp[-\propto_{gw} \cdot \Delta t] + W_{rchrg}(t)\cdot(1 - \exp[-\propto_{gw} \cdot \Delta t]) \tag{6}$$

$$Q_{sb}(t) = \left(\frac{S_{sb}(t)}{K_{sb}}\right)^{\frac{1}{P_{sb}}} \tag{7}$$

$$\frac{dS_{ch}(t)}{dt} = \sum \left(\frac{S_{sb}(t)}{K_{sb}}\right)^{\frac{1}{P_{ch}}} - Q_{ch}(t) \tag{8}$$

$$Q_{ch}(t) = \left(\frac{S_{ch}(t)}{K_{ch}}\right)^{\frac{1}{P_{ch}}} \tag{9}$$

where $S_{sb}(t)$ and $Q_{sb}(t)$ are the storage content and outflow of the storage in the basin and $S_{ch}(t)$ and $Q_{ch}(t)$ the storage content and outflow of the channel at time t, respectively. $Q_{sur}(t)$ and $Q'_{sur}(t)$ are the surface runoff with and without the lag effect consideration at time t; $Q_{surstor}$ is the surface runoff which stored in the watershed at time $t-1$ and surlag is surface runoff lag coefficient. $Q_{lat}(t)$ and $Q'_{lat}(t)$ are the lateral flow with and without the lag effect consideration at time t; $Q_{latstor}$ is the lateral flow which stored in the watershed at time $t-1$ and latlag is lateral flow lag coefficient. $Q_{gw}(t)$ is groundwater flow contributing to the discharge from each sub-basin at time t; $\propto_{gw}$ base flow recession constant; $W_{rchrg}(t)$ is recharge entering the aquifer and Δt is the calculation time interval. K_{sb}, P_{sb}, K_{ch} and P_{ch} are the storage function constants in the basin and channel, respectively.

The input of the SURR model is MAP and Mean Areal Evapotranspiration (MAE) for each of the sub-basins. The observed and forecasted meteorological data can be applied to drive the SURR model for streamflow simulation and forecasting, respectively. The evapotranspiration is calculated using the FAO Penman-Monteith (PM) formula. The FAO PM method is recommended as a standard method for estimating evapotranspiration (ET). The FAO PM method can be expressed as Equation (1):

$$\text{ET} = \frac{0.408\Delta(R_n - G) + \gamma\frac{900}{T+273}u_2(e_s - e_a)}{\Delta + \gamma(1 + 0.34u_2)} \tag{10}$$

where ET is the evapotranspiration (mm day^{-1}), R_n is the net radiation at the crop surface (MJ m^{-2} day^{-1}), G is the soil heat flux density, which is relatively small for daily and ten-day periods (MJ m^{-2} day^{-1}), T is the mean daily air temperature at a height of 2 m ($^\circ$C), u_2 is the wind speed at a height of 2 m (m s^{-1}), e_s is the saturation vapor pressure (KPa), e_a is the actual vapor pressure (KPa), $e_s - e_a$ is the saturation vapor pressure deficit (KPa), Δ is the slope vapor pressure curve (KPa $^\circ$C^{-1}), and γ is the psychrometric constant (KPa $^\circ$C^{-1}). The meteorological data are used to calculate the ET, and then, Thiessen polygons are used by GIS to estimate the MAE for each sub-basin. The rainfall and evapotranspiration data have hourly temporal resolutions, which were spatially interpolated by the Thiessen polygons method using GIS. A detailed description of the SURR model is reported in [42].

The hydrologic models simulate the response of the basin to a given rainfall. Therefore, as an initial assessment, the calibration and verification of the hydrological model could be performed to ensure that the results are accurate and stable. The SURR model was calibrated for the Imjin basin using the observed rainfall and streamflow, and the optimized parameters resulted in a good agreement between the observed and simulated streamflow during the verification periods. The Nash-Sutcliffe Efficiency (NSE) by [44], the Relative Error in Volume (REV) and Kling-Gupta Efficiency (KGE) proposed by [45] were used to compare the results in the calibration and verification periods.

The NSE, REV and KGE equations (following the KGE equation represented in [46]) are as follows:

$$\text{NSE} = 1 - \frac{\sum_{i=1}^{n}(O_i - S_i)^2}{\sum_{i=1}^{n}(O_i - \overline{O})^2} \tag{11}$$

$$\text{REV} = \frac{\sum_{i=1}^{n}S_i - \sum_{i=1}^{n}O_i}{\sum_{i=1}^{n}O_i} \times 100 \tag{12}$$

$$\text{KGE} = 1 - \sqrt{(r-1)^2 + (\propto -1)^2 + (\beta - 1)^2} \tag{13}$$

$$\propto = \frac{\sigma_s}{\sigma_o} \tag{14}$$

$$\beta = \frac{\mu_s}{\mu_o} \tag{15}$$

where O_i is the observed data, S_i is simulated data, $\overline{O}$ is the average of observed data, r is the correlation, $\propto$ is the ratio of the simulation to the observed streamflow standard deviation and β is the ratio of the mean of the simulated and observed streamflow.

The NSE is selected to evaluate the performance of the hydrological model since it shows goodness of fit for the hydrological model. The NSE is a model performance evaluation criterion which is used worldwide. However, the NSE calculates the differences between the observed and simulated streamflow in squared values. This may lead to over- and underestimation of model performance during the high and low flow respectively [47]. Therefore, the REV efficiency criterion is also selected to measure the ratio of the absolute error of the simulated and observed data to the observed data. To overcome the model skill overestimation in NSE criterion the KGE as an alternative metric is selected to measure the hydrological model performance. A comparison between NSE and KGE is

discussed in [45]. The above-mentioned criteria are used to indicate whether the results of the model simulation in calibration and verification process are reasonable or not.

With the NSE range set between 1 (i.e., the ideal value) and negative infinity, values lower than zero indicate that the mean value of the observed streamflow could have better estimate than the model provides. According to the calibration and verification of the SURR model, the results of the streamflow simulations are reasonable and stable with NSEs close to 1. The REV is a measure of precision; it is the ratio of the absolute error of the simulated and observed data to the observed data. The REV can vary among negative infinity to positive infinity and the ideal value is zero. In this study, the results of the calibration and verification for the values of the NSE, REV and KGE showed that the SURR model can well reproduce the observed streamflow in Gunnam, Jeonkuk and Jeogseong stations. The results of the calibration and verification are shown in Table 1.

Table 1. Statistical analysis for the simulated discharge for the calibration and verification periods in the SURR model.

Metric	Calibration Period 23 July–4 September 2007			Calibration Period 1 July–22 August 2008			Verification Period 21 June–4 August 2009		
	Gunnam	Jeonkuk	Jeogseong	Gunnam	Jeonkuk	Jeogseong	Gunnam	Jeonkuk	Jeogseong
NSE	0.69	0.78	0.71	0.70	0.83	0.79	0.57	0.85	0.79
REV	−0.48	−0.12	−0.52	0.37	0.03	0.08	0.16	−0.22	0.03
KGE	0.53	0.62	0.51	0.47	0.85	0.69	0.75	0.68	0.80
Metric	Verification Period 9 July–20 August 2010			Verification Period 16 June–2 August 2011			Verification Period 31 July–13 September 2012		
	Gunnam	Jeonkuk	Jeogseong	Gunnam	Jeonkuk	Jeogseong	Gunnam	Jeonkuk	Jeogseong
NSE	0.62	0.71	0.67	0.71	0.89	0.85	0.59	0.78	0.66
REV	0.23	−0.34	−0.07	−0.09	−0.19	−0.11	−0.28	−0.20	−0.05
KGE	0.42	0.61	0.65	0.87	0.76	0.88	0.47	0.79	0.71

3.3. Bias Correction of Real-Time Forecasts

The NWP models approximate mathematically the physical dynamics using nonlinear differential equations; however, these approximations include uncertainties due to the complex system of the atmosphere [48]. Advancements in meteorological forecast models did not solve the issues related to the inevitable biases. Despite the efforts to incorporate all sources of uncertainty into the forecast and the methodologies applied to generate the forecast ensembles, the results are still subject to errors and systematic biases [49]. Statistical postprocessing increases the accuracy of the forecast data by decreasing the errors. ANN, as a postprocessing method, can determine the complex relationships between the inputs and outputs. ANN has been widely used in the hydrology and modeling of water resource systems [5,12–29].

3.3.1. Description of ANN

ANN is biologically inspired from neurons in the brain and consists of the interaction of computational units. ANN establishes a relationship between the input and target and produces a correct response by following the processes of human brain activities such as saving information, learning, and training [5]. The structure of an ANN includes the input layer (including the input nodes connected to the input variables), hidden layer (it can be one hidden layer or more layers which include the hidden nodes) and output layer (including the output nodes that deliver the output data). Different weights are connected to the nodes (units) of the layers in different forms such as the Feedforward Neural Network (FNN), Convolutional Neural Network (CNN) and Recurrent Neural Networks (RNN). A three-layer FNN is illustrated in Figure 3. Here, i, j and k are the number of nodes for the input, hidden and output layers, respectively. Furthermore, X_i is the input variable, O_j is the output variable, W_{ji} is the connected weight from the input layer to the hidden layer, and W_{kj} is the connected weight from the hidden layer to the output layer. In this study, the FNN is applied to construct the neural network. The weights and bias nodes in the feedforward network are connected in one forward direction.
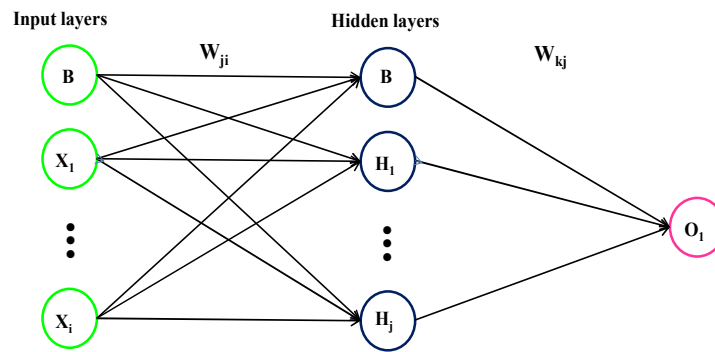
Figure 3. An example schematic of a feedforward network.

ANN is characterized by the simulation and response processes to learn the correct response for each input through training. The general function between input and output is called a transfer (activation) function, which can be a linear or nonlinear function. In this study, the nonlinear sigmoid function is applied for the neural networks. The transfer function converts the summation of the weights (*w*) and inputs (*x*) and (*b*) bias to an output vector by the following equation:

$$y = f(\sum w \times x + b) \tag{16}$$

The inputs are multiplied by weights and then fed to the first hidden layer. The weights can be chosen by minimizing the following error function:

$$E = \frac{1}{2}[Tar_j - O_j(w, x)]^2 \tag{17}$$

where O_j is the output of the output layer and Tar_j is the corresponding target. The procedure of input weight adjustment is called training (learning). In this study, The Levenberg-Marquardt (trainlm) was chosen as the training function and the back propagation generalized delta rule (BPGDR), is applied as the training algorithm that minimizes the error function based on the differences between the modeled and desired outputs. The BPGDR formulation can be summarized in two parts as follows:

1. is for the output weights, which are connected to the output nodes:

$$\Delta w_{kj} = \eta \frac{\partial E}{\partial w_{kj}} \tag{18}$$

2. is for the hidden weights, which are connected to the hidden nodes:

$$\Delta w_{ji} = \eta \frac{\partial E}{\partial w_{ji}} \tag{19}$$

where w_{kj} and the w_{ji} are the output and hidden weights, respectively, *E* is the error function, and η is the learning rate.

3.3.2. Application of ANN for Real-Time Bias Correction

ANN learns the error structure from historical data and corresponding observations. Then, the trained network can be used to reproduce bias-corrected predictions. To apply bias correction in a real-time forecast system, the current time is selected, and the training data set is considered until the current time. The remaining data are then considered as the validation data set. In the training set, the observation is the target, and the forecast is the input data. The objective of using ANN is to find a nonlinear relationship between the input and the target data to achieve the minimum error between the input and target data. A network with few neurons restricts the network learning

ability while one with many neurons may lead to overfitting and poor generalization of the network. Different numbers of the neurons used to construct the model and results showed that by increasing the number of neurons the model performance improved; after 32 neurons the results did not dramatically improved (Figure 4). There are 38 sub-basins in the study area, therefore the 38 neurons were chosen. The stopping criterion used in this study is early stopping; this avoids the overtraining and overfitting of the model for the training data set.
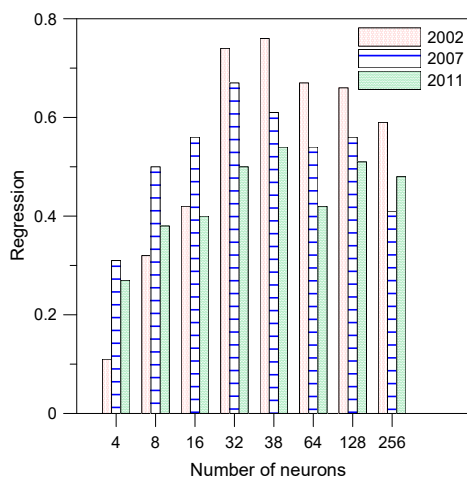

Figure 4. The results of the regression for different number of the neurons.

The schematic of choosing the training and validation data for the ANN construction in this study is provided in Figure 5.
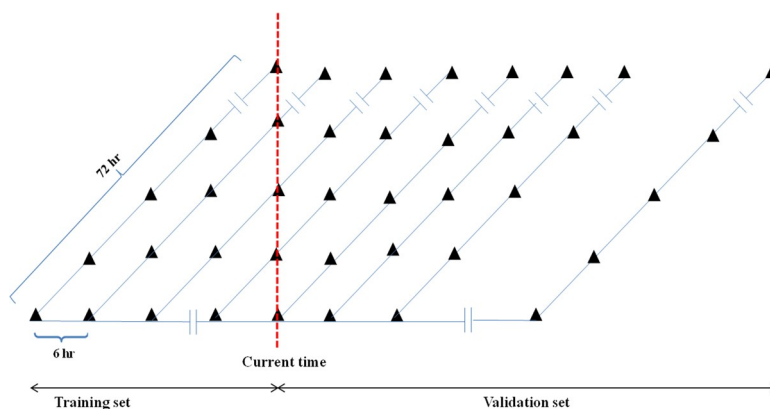

Figure 5. The schematic of the selection of training and validation set data in the real-time forecast of the WRF model output data.

The evaluation criteria used in this study include the Relative Bias (RB), Mean Relative Error (MRE), and the Mean Absolute Error (MAER), as given in Table 2, NSE and REV. In the formulas, O_i is the observed data, and F_i is the forecast data. The RB metric is selected to compare the forecast and observed values by calculating the absolute bias which is normalized by the sum of the observed values. The MRE was also selected to compare the simulated and observed values, the MRE shows the average of the relative error which is the uncertainty of the measurement compared to the measurement. To show the average of the absolute differences between observed and forecast data the MAER was selected to have a comparison between the simulated and observed values.

Table 2. Statistical measures used to evaluate the performance.

Index	Formula
Relative Bias (RB)	$\mathrm{RB} = \dfrac{\sum_{i=1}^{n}(O_i - f_i)}{\sum_{i=1}^{n} O_i}$
Mean Relative Error (MRE)	$\mathrm{MRE} = \dfrac{1}{n} \sum\limits_{i=1}^{n} \dfrac{S_i - O_i}{O_i}$
Mean Absolute Error (MAER)	$\mathrm{MAER} = \dfrac{1}{n} \sum\limits_{i=1}^{n} |O_i - f_i|$

4. Results

4.1. Real-Time Accuracy Improvement of the Precipitation

In real-time flood forecasting, it is undeniable that the accuracy of the real-time precipitation plays the most important role in achieving accurate real-time flood forecasts. In this study, ANN is applied for the bias correction of the real-time precipitation produced by the WRF model. A comparison of the observed rainfall and with/without bias-adjusted real-time WRF rainfall indicated that the accuracy improved with the ANN bias correction (Table 3). The commonly used statistical error measurements such as MRE, RB, REV and MAER compared the skill of model forecasts and observations for error measurement. The results showed that the ANN real-time bias correction improved all statistical terms for the forecast rainfall. A comparison of the results indicated that the use of the bias correction method improved the real-time forecast error measurement statistics by 70.09, 81.61 and 70.49% for the 2002, 2007 and 2011 events, respectively.

Table 3. Results of the improvements to the flood events in 2002, 2007 and 2011.

Event	Forecast data	MRE	RB	REV	MAER
	WRF	38.45	67.73	38.78	114.47
2002	Bias-adjusted WRF	11.64	42.91	7.74	31.17
	Improvement (%)	69.71	57.84	80.05	72.77
	WRF	42.40	35.42	23.20	105.84
2007	Bias-adjusted WRF	10.55	4.03	4.13	20.67
	Improvement (%)	75.12	88.62	82.22	80.47
	WRF	65.61	85.81	61.54	59.83
2011	Bias-adjusted WRF	27.24	13.75	14.82	21.55
	Improvement (%)	58.09	83.98	75.92	63.98

Further investigations are performed to assess the sum, minimum, maximum and percentage of the underestimation of the observed, forecast and bias-corrected forecast rainfall for the 2002, 2007 and 2011 events. Table 4 shows the results of the MAP analysis for the flood events before and after bias correction using ANN. The results obtained before and after real-time ANN bias correction led to an accuracy improvement of MAP by increasing the underestimation and the skill of real-time forecast WRF data. According to the results, after applying the ANN bias correction, the underestimation improved by 65.79, 23.69 and 73.68% for the 2002, 2007 and 2011 events, respectively.

Table 4. Statistics of the MAP for the 2002, 2007 and 2011 flood events.

Event	Data	∑ (mm)	Min (mm)	Max (mm)	Underestimation (%)	Error Reduction (%)
2002	Observation	11100.52	196.19	351.40	-	-
	WRF	6795.70	132.64	246.12	97.37	-
	WRF-revised	11959.45	288.62	362.03	31.58	75.28
2007	Observation	1904.96	299.06	641.59	-	-
	WRF	14622.80	158.51	450.84	78.95	-
	WRF-revised	18255.56	356.49	596.11	55.26	89.53
2011	Observation	17445.92	293.18	743.25	-	-
	WRF	6709.83	52.56	218.64	100	-
	WRF-revised	18021.18	306.21	593.00	34.21	88.74

In the present study, a comparison between the observed and forecast accumulated MAP in all sub-basins is performed to compare the accuracy before and after bias correction. It is evident from Figure 6 that after bias correction, the accumulated WRF data have improved significantly. The scatterplot of the observed, real-time, and bias-corrected real-time forecast MAP indicated that the ANN bias correction method applied to the Imjin basin increased the real-time forecast accuracy by decreasing the underestimation of the precipitation in all the sub-basins. A comparison of the results of the accumulated observed rainfall and the real-time forecast WRF data showed that the ANN bias correction method used in this study was able to reduce the biases of real-time precipitation with the desired accuracy.
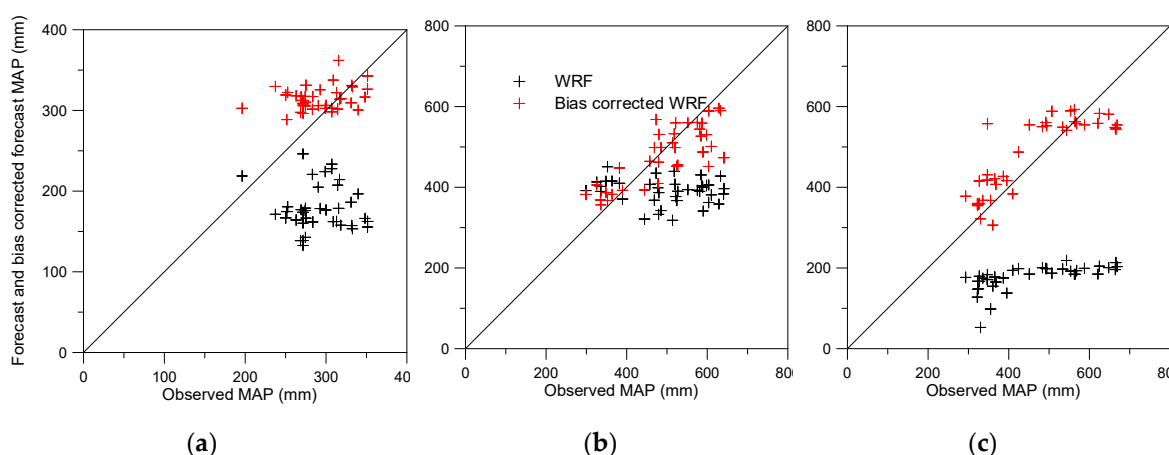
Figure 6. The scatterplot of the accumulated observed MAP and mean ensemble of real-time WRF data before and after bias correction for the events in (**a**) 2002, (**b**) 2007 and (**c**) 2011.
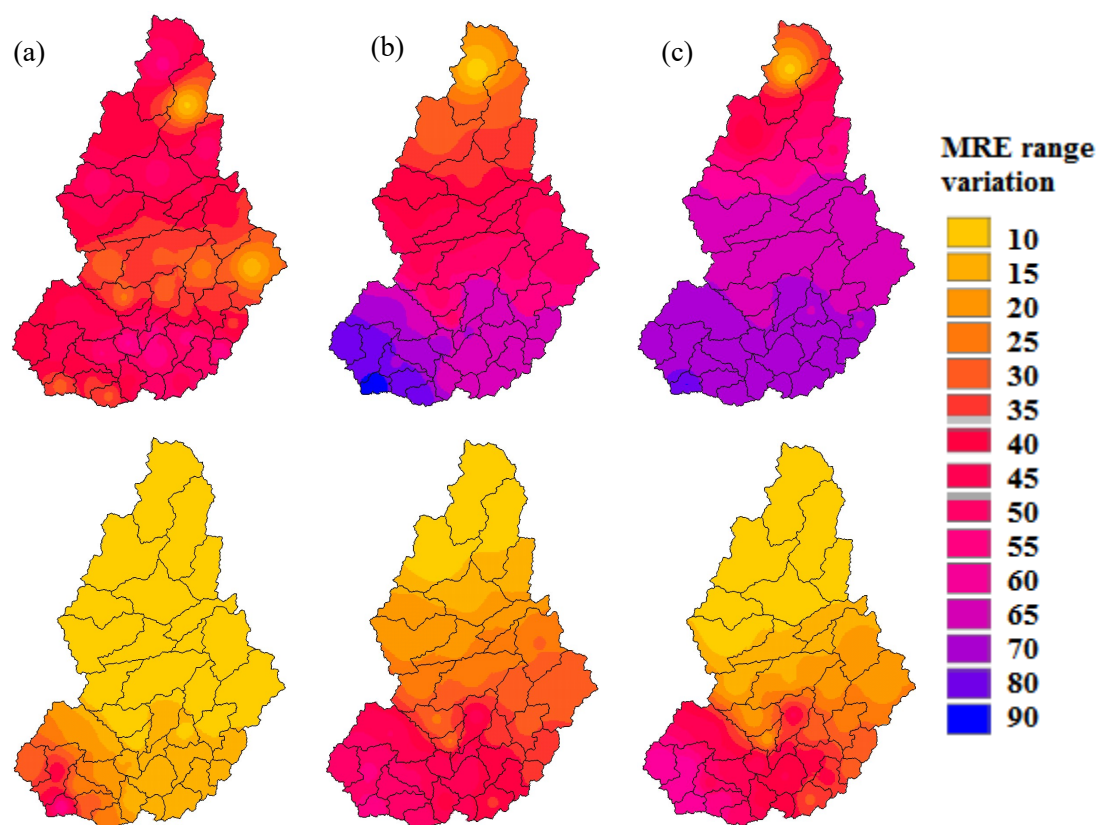
The spatial distribution of the MRE on the catchment scale indicted that the ANN bias correction led to a decrease of the MAER in all the sub-basins (Figure 7). The results of the MRE assessment of the 38 sub-basins indicated that the error reduction of the forecast MAP varies by sub-basin in the study area. The results of the ANN real-time bias correction showed that the average improvements of the MRE over the catchment are 69.71, 61.24 and 53.90% for the 2002, 2007 and 2011 events, respectively. By applying the forecast bias correction, the forecast capability and the accuracy of the model predictions improved remarkably.

4.2. Real-Time Flood Forecasting Accuracy Improvement

In this section, the real-time flood forecast accuracy evaluation is performed by comparing the observed, simulated and forecasted values. The simulation floods were estimated using the observation MAP as input to the SURR model, while the forecast was obtained using the real-time WRF data as the input to the SURR model. The statistical error measurements (NSE, KGE, MRE and REV) were used to

compare the performance of hydrologic simulations and forecasts before and after bias correction and determine the average deviations.

In this study, we used gauge and WRF precipitation data to drive the hydrological model to simulate and forecast flood events. Here, the 72-h real-time forecast data at a spatial resolution of 1 km × 1 km and a temporal resolution of 10 min are used as input to the SURR model over the Imjin basin; furthermore, the bias-corrected WRF data are used as the input data for the SURR model. The coupling system of the SURR and WRF model includes the use of the observed precipitation until the start of the forecast time, and then continues to apply the WRF data for a 72-h forecast lead time. The observed and real-time WRF data (bias-corrected and raw data) are used to run the hydrological model, and this process is repeated for the next 6 h to the end of the forecast time. Among the various forecast ensembles, only one stream flow forecast is shown with the relevant precipitation to indicate the real-time forecast discharge variation over time due to space limitations. According to the findings of this study, by applying the bias-adjusted WRF data, the accuracy improvement was suggested by the increasing NSE and KGE and decreasing MRE and REV (Table 5).


Figure 7. The comparison of the spatial distribution of the MRE in 38 sub-basins before (upper part) and after bias correction (down part) for the events in (**a**) 2002, (**b**) 2007 and (**c**) 2011.

The performance of the SURR model in simulating the streamflow along with the SURR-WRF coupled model before and after bias correction in forecasting the streamflow at the Gunnam, Jeonkuk and Jeogseong stations in the 2002, 2007 and 2011 events are illustrated in Figure 8. The observed stream flow (black dashed curve), the forecast stream flow using WRF data (blue curve), the forecast stream flow using bias-corrected WRF data (green curve) and the simulated streamflow (red curve) are presented in Figure 8. The Jeonkuk station has no observation data for the 2002 event.

Table 5. Comparison of results for the statistical error measurement for the 2002, 2007 and 2011 events.

Index	Station	SURR	SURR-WRF	SURR-Revised WRF	Improvement (%)
			Event 2002		
NSE		0.26	−18.27	−7.24	60.21
MRE	Gunnam	−0.09	−0.95	−0.24	74.74
REV		0.16	0.70	0.43	38.57
KGE		0.41	−1.20	−0.52	56.67
NSE		0.68	−19.85	−8.68	56.27
MRE	Jeogseong	−0.25	0.80	0.26	67.50
REV		0.03	0.53	0.27	49.06
KGE		0.60	−1.14	−0.68	40.35
			Event 2007		
NSE		0.69	−4.57	−2.01	56.02
MRE	Gunnam	−0.58	−0.60	−0.56	6.67
REV		−0.48	−0.57	−0.52	8.77
KGE		0.53	−5.03	−3.98	20.87
NSE		0.78	−6.63	−0.82	87.63
MRE	Jeonkuk	−0.60	−0.77	−0.37	51.95
REV		−0.12	−0.22	−0.18	18.18
KGE		0.62	−2.77	−1.65	40.43
NSE		0.71	−10.30	−5.71	44.56
MRE	Jeogseong	−0.69	−0.78	−0.65	16.67
REV		−0.52	−0.54	−0.59	9.26
KGE		0.51	−3.30	−2.24	32.12
			Event 2011		
NSE		0.80	−0.47	0.07	85.11
MRE	Gunnam	−0.49	−0.79	−0.51	35.44
REV		−0.08	−0.59	−0.37	37.29
KGE		0.81	−0.26	−0.09	65.38
NSE		0.81	−0.87	−0.06	93.10
MRE	Jeonkuk	−0.63	−0.67	−0.58	13.43
REV		−0.34	−0.73	−0.42	42.47
KGE		0.60	−0.79	−0.21	73.42
NSE		0.90	−1.06	−0.23	78.30
MRE	Jeogseong	−0.06	−0.56	−0.07	87.50
REV		−0.45	−0.60	−0.32	46.67
KGE		0.81	−1.22	−0.46	62.29

The observed and real-time forecast precipitation (with/without bias correction) events are shown separately in different panels. Comparing the flood observation and simulation, the rising and falling limb and amplitude of the simulated flood, which used observed precipitation, is quite similar to the observations, while the forecasted flood by the WRF model followed similar trend by significant underestimation. This result can be explained by the fact that observation and real-time forecast precipitation are two various sources of input data that are forced into the SURR model.
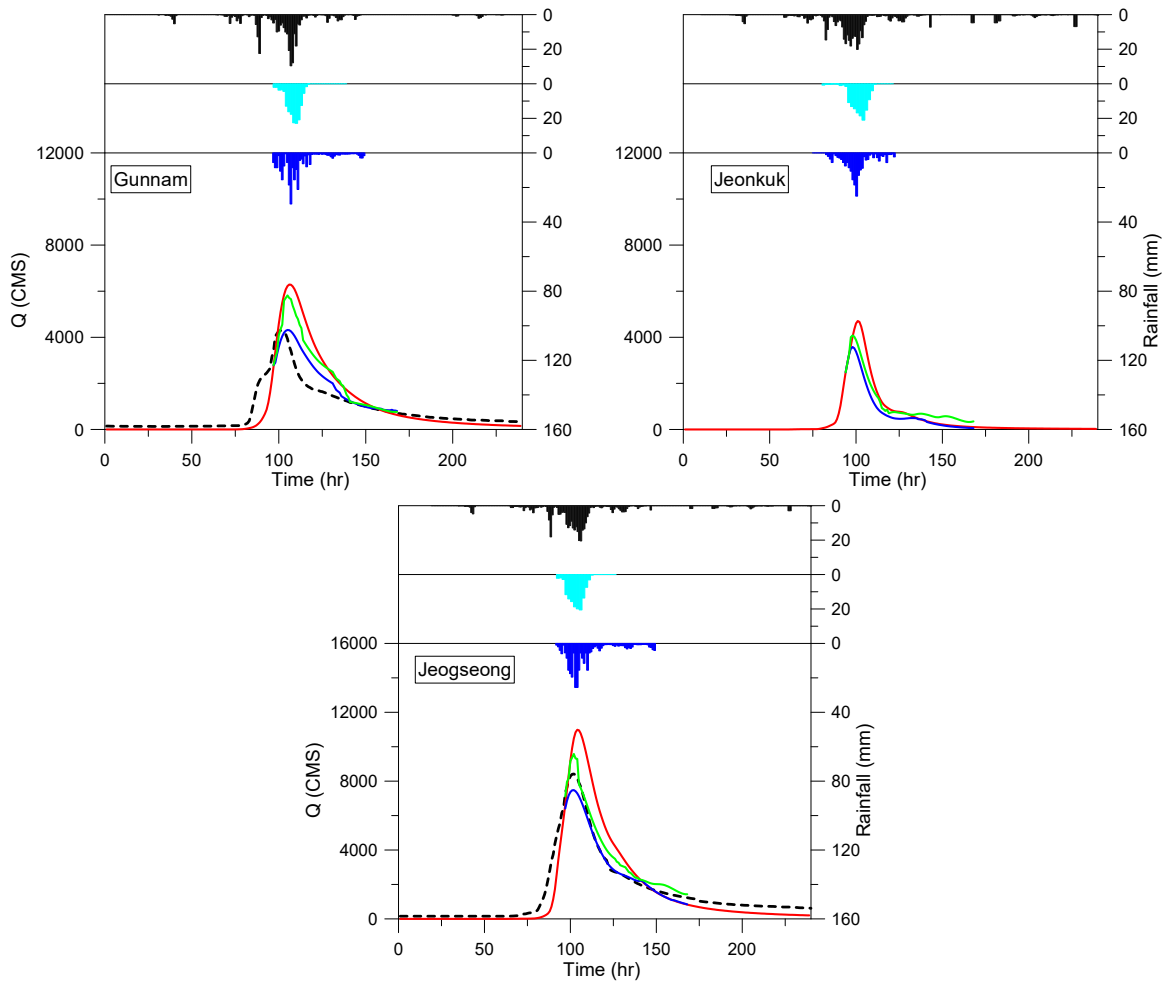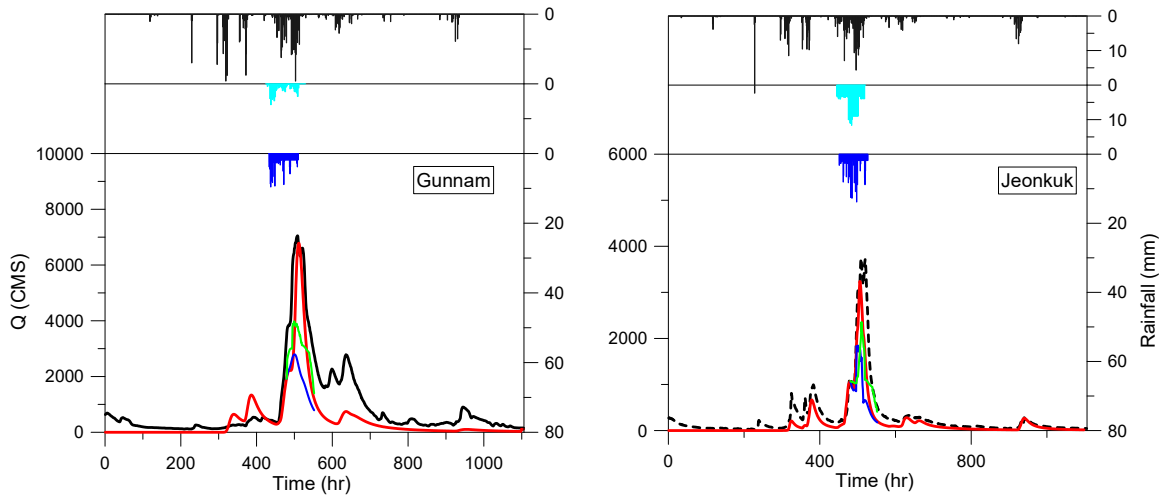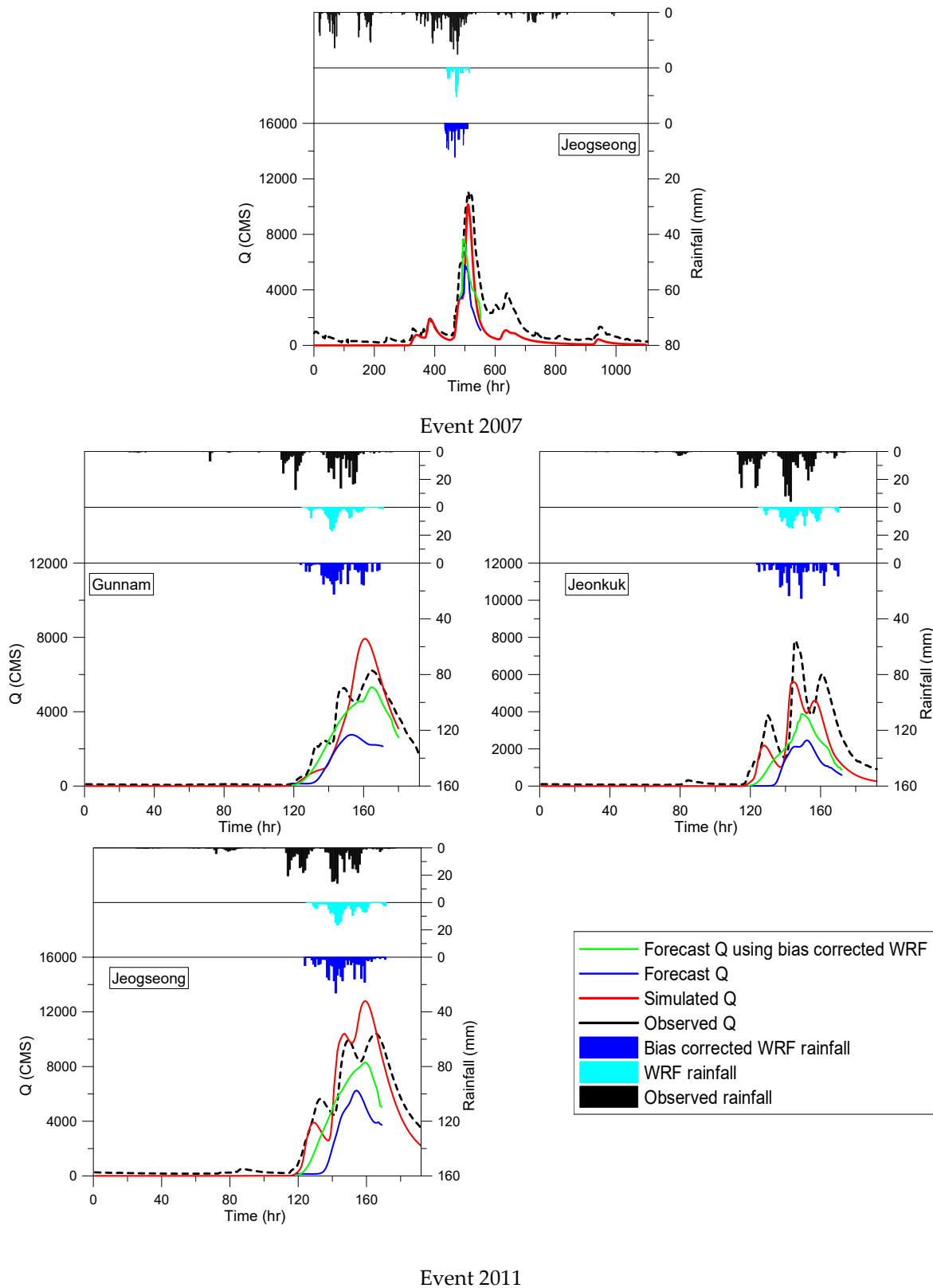
Event 2002

Figure 8. *Cont.*

Event 2007

Event 2011

Figure 8. Comparison of simulated, observed and forecasted flows (before and after bias correction) and observed and forecasted rainfall (before and after bias correction) for 2002, 2007 and 2011 events.

5. Discussion

The NWP models determine the future state of the weather by forcing current weather conditions into the atmospheric models. The chaotic and nonlinear system of the atmosphere and complex nature of precipitation made precipitation difficult to forecast accurately with the NWP models. In general, the NWP models forecast less accurate precipitation rates than indicated by the observed precipitation rates. The precipitation intensity [50] and location [51] are challenging for precipitation forecasting. The initial and boundary conditions such as horizontal resolution, domain size as grid spacing and physical parameterization schemes are directly related to the NWP model results in heavy precipitation forecasting [37,52]. The Quantitative Precipitation Forecast (QPF) accuracy in three-dimensional primitive-equation atmosphere circulation models, such as WRF, can be influenced by different initializations, microphysics, and planetary boundary layer (PBL) schemes [53]. In this study, the WRF real-time forecast data, in comparison with the observed data, had systematic biases; the errors related to the NWP model forecasts were reflected in the underestimation of the real-time precipitation forecast by the WRF model. The cumulative MAP had the underestimations of 97.37, 78.95 and 100% for the 2002, 2007 and 2011 events, respectively. Because the Imjin River is a transboundary river, a reliable streamflow forecast is needed for this watershed. Improving the streamflow forecast in the Imjin basin is a highly important task especially during heavy rainfall and extreme events. For a reliable flood forecast, an accurate forecast of rainfall is needed, but the use of raw WRF data caused large biases in the flood forecast.

The aim of the present study is to improve real-time flood forecasting by applying ANN as a postprocessing technique. Considering all real-time forecast cases, it can be concluded that on average, hydrological forecasts based on the WRF model forecast reproduced stream flow with a significant underestimation. ANN was able to construct a relationship between the input and output data to reduce the biases between the observed and forecast rainfall data. Therefore, the use of the ANN bias correction resulted in the improvement of the real-time flood forecasts in the Imjin basin for the Gunnam, Jeonkuk and Jeogseong stations. By applying the ANN bias correction, errors in precipitation forecasts are modified, which resulted in the real-time precipitation forecast accuracy enhancement, which is not uniform over the forecast interval. The results indicated that there was significant improvement in the statistical errors in the forecast MAP before and after applying the bias correction method. By using the ANN bias correction, the underestimation of the real-time forecast data and the accumulated forecast MAP improved by 65.57, 30.03 and 65.79% for the 2002, 2007 and 2011 events, respectively. The use of the bias-corrected precipitation resulted in the significant improvement in the real-time flood forecasting by 57.53, 33.31 and 57.70% for the 2002, 2007 and 2011 events, respectively. The promising results indicated that the ANN bias correction in the Imjin River had resulted in the improved performance of real-time flood forecasting.

The forecast verification indicated a noteworthy increase in forecast performance with ANN, compared to the raw model outputs. The precipitation real-time forecast accuracy enhancement can translate to the improvement in real-time flood forecasts. However, the results of the real-time flood forecasts were still underestimated because a perfect estimate of real-time forecast rainfall quantity is not easily obtained. This complexity is the result of the two sources of precipitation, which are quite different. The spatial and temporal variation in the rainfall characteristics were not captured well by the WRF model in the real-time forecast data. Typically, the forecasted floods underestimated the peak floods, and the forecasted flood errors are related to the inaccuracies in the real-time forecasted rainfall. Considering all real-time forecast cases from the start of the forecasting time until the end of the forecasting time, on average, it can be concluded that hydrological forecasts based on meteorological model inputs were able to reproduce the shape and the timing of the calculated stream flow fairly well. However, the underestimation of the WRF model bias-corrected precipitation was affected by the real-time forecast discharge in all events. Another reason for the uncertainties in real-time flood forecasting after bias correction could be related to the fact that the hydrological model calibration was performed with rain gauge data and observed streamflow data; however, the coupled SURR-WRF

model used the real-time forecasted rainfall. These different sources of rainfall were used as inputs for the hydrological models. Therefore, it could be expected that the hydrological response in forecasting the streamflow would not match the simulated streamflow very well. For the real-time flood forecasts, although the real-time flood forecasts are not perfectly matched the observed values even after applying the bias correction, available forecast data are preferred over completely ignoring future events of interest. Due to the importance of the Imjin basin for both North and South Korea, available information regarding flood forecasts in the studied area is valuable.

6. Conclusions and Recommendations

In hydrometeorological studies, the performance of coupled hydrometeorological models is directly dependent on the accuracy of the forecasted precipitation. Because the NWP models cannot forecast precipitation accurately, postprocessing of the output of NWP models is necessary. The postprocessing of the real-time systems can be performed using historical data and forecasts by ANN bias correction. In this study, ANN is applied for the bias correction of the real-time forecast of the WRF model. The bias correction is estimated to quantify the accuracy improvement of the rainfall and corresponding flood forecasts in a transboundary river. The main conclusions of this study are summarized below:

(1) Applying ANN for bias correction improved the forecast performance by reducing MRE, RB, REV and MAER by 69.71, 57.84, 80.05 and 72.77%, respectively, in the 2002 event; by 75.12, 88.62, 82.22 and 80.47%, respectively, in the 2007 event; and by 58.09, 83.98, 75.92 and 63.98%, respectively, in the 2011 event.
(2) The sum, minimum, maximum and the underestimation of the WRF real-time forecast data were improved after applying the ANN bias correction to the real-time WRF data.
(3) By applying the ANN bias correction, the underestimation of WRF data improved 65.79, 23.69 and 73.68% in the 2002, 2007 and 2011 events, respectively. The error was also reduced by 75.28, 89.53 and 88.74% over the Imjin catchment in terms of the accumulated MAP in the 2002, 2007 and 2011 events, respectively.
(4) The error comparison in each sub-basin indicated that the average percentage of MRE reduction in the catchment was 69.71, 61.24 and 53.90% for the 2002, 2007 and 2011 events, respectively.
(5) By applying the ANN bias correction, the performance of the SURR-WRF coupled models in real-time flood forecasts increased by increasing the NSE and KGE and reducing the MRE and REV for Gunnam, Jeonkuk and Jeogseong stations.

Additional analyses could be performed to compare the benefits of using different QPF postprocessing techniques such as radar data assimilation, regression methods and Kalman filtering.

Author Contributions: Conceptualization, J.A. and B.D-H.; Data curation, J.A.; Formal analysis, J.A.; Funding acquisition, B.D-H.; Methodology, A.J.; Project administration, B.D-H.; Resources, J.A. and B.D-H.; Supervision, B.D-H.; Validation, J.A.; Visualization, J.A. and B.D-H.; Writing—original draft, J.A.; Writing—review & editing, J.A. and B.D-H.

Conflicts of Interest: The authors declare no conflict of interest.

References

1. Liu, J.; Wang, J.; Pan, S.; Tang, K.; Li, C.; Han, D. A real-time flood forecasting system with dual updating of the NWP rainfall and the river flow. *Nat. Hazards* **2015**, *77*, 1161–1182. [CrossRef]
2. Vincendon, B.; Ducrocq, V.; Nuissier, O.; Vie', B. Perturbation of convection-permitting NWP forecasts for flash-flood ensemble forecasting. *Nat. Hazards Earth Syst. Sci.* **2011**, *11*, 1529–1544. [CrossRef]

3.   Lin, C.A.; Wen, L.; Lu, G.; Wu, Z.; Zhang, J.; Yang, Y.; Zhu, Y.; Tong, L. Real-time forecast of the 2005 and 2007 summer severe floods in the Huaihe River Basin of China. *J. Hydrol.* **2010**, *381*, 33–41. [CrossRef]

4.   Davolio, S.; Miglietta, M.M.; Diomede, T.; Marsigli, C.; Montani, A. A flood episode in northern Italy: Multi-model and single-model mesoscale meteorological ensembles for hydrological predictions. *Hydrol. Earth Syst. Sci.* **2013**, *17*, 2107–2120. [CrossRef]

5.   Moghim, S.; Bras, R.L. Bias Correction of Climate Modeled Temperature and Precipitation Using Artificial Neural Networks. *J. Hydrometeor.* **2017**, *18*, 1867–1884. [CrossRef]

6.   Yang, Z.; Hsu, K.; Sorooshian, S.; Xu, X.; Braithwaite, D.; Verbist, K.M.J. Bias Adjustment of Satellite-based Precipitation Estimation using Gauge Observations-A Case Study in Chile. *J. Geophys. Res.-Atmos.* **2016**, *121*, 3790–3806. [CrossRef]

7.   Crochemore, L.; Ramos, M.H.; Pappenberger, F. Bias correcting precipitation forecasts to improve the skill of seasonal streamflow forecasts. *Hydrol. Earth Syst. Sci.* **2016**, *20*, 3601–3618. [CrossRef]

8.   Rogelis, M.C.; Werner, M. Streamflow forecasts from WRF precipitation for flood early warning in mountain tropical areas. *Hydrol. Earth Syst. Sci.* **2017**, *22*, 853–870. [CrossRef]

9.   Applequist, S.; Garhs, G.; Pfeffer, R. Comparisons of methodologies for probabilistic quantitative precipitation forecasting. *Weather Forecast.* **2002**, *17*, 783–799. [CrossRef]

10.   Charba, J.; Samplatsky, F. High-resolution GFS-based MOS quantitative precipitation forecasts on a 4-km grid. *Mon. Weather Rev.* **2011**, *139*, 39–68. [CrossRef]

11.   Cane, D.; Ghigo, S.; Rabuffetti, D.; Milelli, D. Real-time flood forecasting coupling different post processing techniques of precipitation forecast ensembles with a distributed hydrological model. The case study of May 2008 flood in western Piemonte, Italy. *Nat. Hazards Earth Syst. Sci.* **2013**, *13*, 211–220. [CrossRef]

12.   Chen, J.; Brissette, F.P.; Chaumont, D.; Braun, M. Finding appropriate bias correction methods in downscaling precipitation for hydrologic impact studies over North America. *Water Resour. Res.* **2013**, *49*, 4187–4205. [CrossRef]

13.   Tapiador, F.J.; Kidd, C.; Hsu, K.-L.; Marzano, F.S. Neural networks in satellite rainfall estimation. *Meteorol. Appl.* **2004**, *11*, 83–91. [CrossRef]

14.   Hsu, K.; Gao, H.; Soroshian, S.; Gupta, H. Precipitation estimation from remotely sensed information using artificial neural networks. *J. Appl. Meteorol. Climatol.* **1997**, *36*, 1176–1190. [CrossRef]

15.   Rivolta, G.; Marzano, F.S.; Coppola, E.; Verdecchia, M. Artificial neural-network technique for precipitation nowcasting from satellite imagery. *Adv. Geosci.* **2006**, *7*, 97–103. [CrossRef]

16.   Aichouri, I.; Hani, A.; Bougherira, N.; Djabri, L.; Chaffai, H.; Lallahem, S. River flow model using artificial neural networks. *Energy Proced.* **2015**, *74*, 1007–1014. [CrossRef]

17.   Wu, C.L.; Chau, K.W. Rainfall–runoff modeling using artificial neural network coupled with singular spectrum analysis. *J. Hydrol.* **2011**, *399*, 394–409. [CrossRef]

18.   Peng, T.; Zhou, J.; Zhang, C.; Fu, W. Streamflow forecasting using empirical wavelet transform and artificial neural networks. *Water* **2017**, *9*, 406. [CrossRef]

19.   Wang, Y.; Min, J.; Chen, Y.; Xiang-Yu, H.; Zeng, M.; Li, X. Improving precipitation forecast with hybrid 3DVar and time-lagged ensembles in a heavy rainfall event. *Atmos. Res.* **2017**, *183*, 1–16. [CrossRef]

20.   Chiang, Y.M.; Chang, F.J. Integrating hydrometeorological information for rainfall–runoff modelling by artificial neural networks. *Hydrol Process.* **2009**, *23*, 1650–1659. [CrossRef]

21.   Ahmad, S.; Simonovic, S.P. An artificial neural network model for generating hydrograph from hydro-meteorological parameters. *J. Hydrol.* **2005**, *315*, 236–251. [CrossRef]

22.   Chang, F.J.; Tsai, M.J. A nonlinear spatio-temporal lumping of radar rainfall for modeling multi-step-ahead inflow forecasts by data-driven techniques. *J. Hydrol.* **2016**, *535*, 256–269. [CrossRef]

23.   Tayfur, G.; Singh, V.P.; Moramarco, T.; Barbetta, S. Flood Hydrograph Prediction Using Machine Learning Methods. *Water* **2018**, *10*, 968. [CrossRef]

24.   Zhou, J.; Peng, T.; Zhang, C.; Sun, N. Data Pre-Analysis and Ensemble of Various Artificial Neural Networks for Monthly Streamflow Forecasting. *Water* **2018**, *10*, 628. [CrossRef]

25.   Chang, L.-C.; Amin, M.Z.M.; Yang, S.-N.; Chang, F.-J. Building ANN-Based Regional Multi-Step-Ahead Flood Inundation Forecast Models. *Water* **2018**, *10*, 1283. [CrossRef]

26.   Chang, L.C.; Shen, H.Y.; Chang, F.J. Regional flood inundation nowcast using hybrid SOM and dynamic neural networks. *J. Hydrol.* **2014**, *519*, 476–489. [CrossRef]

27. Tien Bui, D.; Khosravi, K.; Li, S.; Shahabi, H.; Panahi, M.; Singh, V.P.; Chapi, K.; Shirzadi, A.; Panahi, S.; Chen, W.; et al. New Hybrids of ANFIS with Several Optimization Algorithms for Flood Susceptibility Modeling. *Water* **2018**, *10*, 1210. [CrossRef]

28. Maier, H.R.; Dandy, G.C. Neural networks for the prediction and forecasting of water resources variables: A review of modelling issues and applications. *Environ. Model. Softw.* **2000**, *15*, 101–124. [CrossRef]

29. Maier, H.R.; Jain, A.; Dandy, G.C.; Sudheer, K.P. Methods used for the development of neural networks for the prediction of water resource variables in river systems: Current status and future directions. *Environ. Model. Softw.* **2010**, *25*, 891–909. [CrossRef]

30. Singh, P.; Borah, B. Indian summer monsoon rainfall prediction using artificial neural network. *Stoch. Environ. Res. Risk Assess* **2013**, *27*, 1585–1599. [CrossRef]

31. Maier, H.R.; Kapelan, Z.; Kasprzyk, J.; Kollat, J.; Matott, L.S.; Cunha, M.C.; Dandy, G.C.; Gibbs, M.S.; Keedwell, E.; Marchi, A.; et al. Evolutionary algorithms and other metaheuristics in water resources: Current status, research challenges and future directions. *Environ. Model. Softw.* **2014**, *62*, 271–299. [CrossRef]

32. Lee, S.; Bae, D.H.; Cho, C.H. Changes in future precipitation over South Korea using a global high-resolution climate model. *Asia-Pac. J. Atmos. Sci.* **2013**, *49*, 619–624. [CrossRef]

33. Lee, J.; Choi, J.; Lee, O.; Yoon, J.; Kim, S. Estimation of Probable Maximum Precipitation in Korea using a Regional Climate Model. *Water* **2017**, *9*, 240. [CrossRef]

34. Kim, N.W.; Won, Y.S.; Chung, I.M. The scale of typhoon RUSA. *Hydrol. Earth Syst. Sci.* **2006**, *3*, 3147–3182. [CrossRef]

35. You, C.H.; Lee, D.I.; Jang, S.M.; Jang, M.; Uyeda, U.; Shinoda, Y.; Kobayashi, F. Characteristics of rainfall systems accompanied with Changma front at Chujado in Korea. *ASIA-Pac. J. Atmos. Sci.* **2010**, *46*, 41–51. [CrossRef]

36. Kim, E.; Ra, I.; Rhee, K.H.; Kim, C.S. Estimation of real-time flood risk on roads based on rainfall calculated by the revised method of missing rainfall. *Sustainability* **2014**, *6*, 6418–6431. [CrossRef]

37. Jee, J.-B.; Kim, S. Sensitivity Study on High-Resolution WRF Precipitation Forecast for a Heavy Rainfall Event. *Atmosphere* **2017**, *8*, 96. [CrossRef]

38. Yucel, I.; Onen, A.; Yilmaz, K.; Gochis, D. Calibration and evaluation of a flood forecasting system: Utility of numerical weather prediction model, data assimilation and satellite-based rainfall. *J. Hydrol.* **2015**, *523*, 49–66. [CrossRef]

39. Lee, D.K.; Eom, D.Y.; Kim, J.W.; Lee, J.B. High-resolution summer rainfall prediction in the JHWC real-time WRF system. *Asia-Pac. J. Atmos. Sci.* **2010**, *46*, 341–353. [CrossRef]

40. Srivastava, P.K.; Han, D.; Rico-Ramirez, M.A.; O'Neill, P.; Islam, T.; Gupta, M.; Dai, Q. Performance evaluation of WRF-Noah Land surface model estimated soil moisture for hydrological application: Synergistic evaluation using SMOS retrieved soil moisture. *J. Hydrol.* **2015**, *529*, 200–212. [CrossRef]

41. Skamarock, W.C.; Klemp, J.B.; Dudhia, J.; Gill, D.O.; Barker, D.M.; Duda, G.; Huang, X.; Wang, W.; Powers, J.G. *A Description of the Advanced Research WRF Version 3*; Tech. Note, NCAR/TN-475+STR; National Center for Atmospheric Research: Boulder, CO, USA, 2008.

42. Bae, D.H.; Lee, B.J. Development of Continuous Rainfall Runoff Model for Flood Forecasting on the Large Scale Basin. *J. Korea Water Resour. Assoc.* **2011**, *44*, 51–64. [CrossRef]

43. Kimura, T. *The Flood Runoff Analysis Method by the Storage Function Model*; The Public Works Research Institute Ministry of Construction: Tsukuba, Japan, 1961.

44. Nash, J.E.; Sutcliffe, J.V. River flow forecasting through. Part, I. A conceptual model discussion of principles. *J. Hydrol.* **1970**, *10*, 282–290. [CrossRef]

45. Gupta, H.V.; Kling, H.; Yilmaz, K.K.; Martinez, G.F. Decomposition of the mean squared error and nse performance criteria: Implications for improving hydrological modelling. *J. Hydrol.* **2009**, *377*, 80–91. [CrossRef]

46. Seo, B.C.; Quintero, F.; Krajewski, F.W. High-Resolution QPF Uncertainty and Its Implications for Flood Prediction: A Case Study for the Eastern Iowa Flood of 2016. *J. Hydrometeor.* **2016**, *19*, 1289–1304. [CrossRef]

47. Krause, P.; Boyle, D.P.; Bäse, F. Comparison of different efficiency criteria for hydrological model assessment. *Adv. Geosci.* **2005**, *5*, 89–97. [CrossRef]

48. Cloke, H.L.; Pappenberger, F. Ensemble flood forecasting: A review. *J. Hydrol.* **2009**, *375*, 613–626. [CrossRef]

49. Madadgar, S.; Moradkhani, H.; Garen, D. Towards improved post-processing of hydrologic forecast ensembles. *Hydrol. Process.* **2012**, *28*, 104–122. [CrossRef]

50. Kobold, M.; Suselj, K. Precipitation forecasts and their uncertainty as input into hydrological models. *Hydrol. Earth Syst. Sci.* **2005**, *9*, 322–332. [CrossRef]

51. Ebert, E.; McBride, J. Verification of precipitation in weather systems: Determination of systematic errors. *J. Hydrol.* **2000**, *239*, 179–202. [CrossRef]

52. Wang, X.; Steinle, P.; Seed, A.; Xiao, Y. The Sensitivity of Heavy Precipitation to Horizontal Resolution, Domain Size, and Rain Rate Assimilation: Case Studies with a Convection-Permitting Model. *Adv. Meteorol.* **2016**, *2016*, 7943845. [CrossRef]

53. Jankov, I.; Gallus, W.A.; Segal, M.; Koch, S.E. Influence of Initial Conditions on the WRF–ARW Model QPF Response to Physical Parameterization Changes. *Weather Forecast.* **2007**, *22*, 501–519. [CrossRef]